APPLIED AND ENVIRONMENTAL MICROBIOLOGY, Aug. 2001, p. 3683–3692 Vol. 67, No. 8
0099-2240/01/$04.00+0 DOI: 10.1128/AEM.67.8.3683–3692.2001

Cluster Structure of Anaerobic Aggregates of an Expanded Granular Sludge Bed Reactor

G. GONZALEZ-GIL,[1]* P. N. L. LENS,[1,2] A. VAN AELST,[3] H. VAN AS,[2] A. I. VERSPRILLE,[4] AND G. LETTINGA[1]

Sub-department of Environmental Technology,[1] Department of Molecular Physics,[2] and Department of Plant Cytology and Morphology,[3] University of Wageningen, 6700 EV Wageningen, and Biothane Systems International, 2600 GB Delft,[4] The Netherlands

Received 18 January 2001/Accepted 4 May 2001

The metabolic properties and ultrastructure of mesophilic aggregates from a full-scale expanded granular sludge bed reactor treating brewery wastewater are described. The aggregates had a very high methanogenic activity on acetate (17.19 mmol of CH_4/g of volatile suspended solids [VSS]·day or 1.1 g of CH_4 chemical oxygen demand/g of VSS·day). Fluorescent in situ hybridization using 16S rRNA probes of crushed granules showed that 70 and 30% of the cells belonged to the archaebacterial and eubacterial domains, respectively. The spherical aggregates were black but contained numerous whitish spots on their surfaces. Cross-sectioning these aggregates revealed that the white spots appeared to be white clusters embedded in a black matrix. The white clusters were found to develop simultaneously with the increase in diameter. Energy-dispersed X-ray analysis and back-scattered electron microscopy showed that the whitish clusters contained mainly organic matter and no inorganic calcium precipitates. The white clusters had a higher density than the black matrix, as evidenced by the denser cell arrangement observed by high-magnification electron microscopy and the significantly higher effective diffusion coefficient determined by nuclear magnetic resonance imaging. High-magnification electron microscopy indicated a segregation of acetate-utilizing methanogens (*Methanosaeta* spp.) in the white clusters from syntrophic species and hydrogenotrophic methanogens (*Methanobacterium*-like and *Methanospirillum*-like organisms) in the black matrix. A number of physical and microbial ecology reasons for the observed structure are proposed, including the advantage of segregation for high-rate degradation of syntrophic substrates.

The view of the structure of biofilms has dramatically changed during the last decade. Until the early 1990s, biofilms were considered more or less homogeneous layers of microorganisms embedded in a matrix of extracellular polymeric substances (23, 32). The application of one-dimensional models to calculate concentration profiles in these biofilms is straightforward. In general, an excellent agreement between observed concentration gradients (16) and predicted ones was obtained using one-dimensional models (34) for the biofilm systems studied.

More-detailed investigations using advanced microscopic techniques revealed that biofilm morphology can be much more complex. Confocal scanning laser microscopy and computerized image analysis tools were used to show that glucose-grown *P. aeruginosa* biofilms were composed of cell clusters separated by interstitial voids and channels (6, 7, 26, 39, 46). Based on these observations, biofilms containing these clusters were referred to as having a cluster-and-channel morphology and the clusters were visualized as "mushrooms" (3). Also other aerobic, multispecies biofilms have been found to contain a structured cell cluster-and-channel arrangement (10).

Anaerobic aggregates from anaerobic wastewater treatment plants are a special type of biofilms. These spherical biofilms are formed spontaneously by autoimmobilization of anaerobic bacteria in the absence of a support material (22). The view on the structure of anaerobic granular sludge has also substantially changed in the last decade. In the early 1990s, it was questioned whether anaerobic aggregates have a homogeneous or heterogeneous structure. Several microscopic, molecular, and microsensor tools were used to document well the heterogeneous structure of upflow anaerobic sludge bed (UASB) aggregates (14, 15, 21, 24). However, aggregates with a homogeneous structure have also been described (8, 12). The observed heterogeneous structure in aggregates was mainly related to the presence of concentric biomass layers with different metabolic activities (24). Methanogenic activity is predominantly located in the core of the aggregates, around which layers with predominantly fermentative (21, 24) or sulfate-reducing (34, 37) activity are present.

Thus far, the cluster morphology for anaerobic aggregates or biofilms has not, to the best of our knowledge, been reported. During a study of the quality of anaerobic aggregates developing in full-scale expanded granular sludge bed (EGSB) reactors, aggregates with a clear cluster structure were observed in an EGSB reactor treating brewery wastewater. Compared to UASB reactors, EGSB reactors operate at much higher liquid upflow velocities (6 to 10 m/h versus 0.5 to 2 m/h). The special design of the three-phase separator allows a much higher hydraulic load than that achieved in UASB systems, and hence they can be operated as high-loaded reactors up to 30 kg of chemical oxygen demand (COD) per m^3 of reactor per day (22, 27, 48).

* Corresponding author. Mailing address: Sub-department of Environmental Technology, University of Wageningen, Bomenweg 2, P.O. Box 8129, 6700 EV Wageningen, The Netherlands. Phone: 31 (0) 317 485595. Fax: 31 (0) 317 482108. E-mail: graciela.gonzalez@algemeen.mt.wau.nl.

TABLE 1. Main chemical composition of the brewery wastewater on which the granular sludge was grown

Parameter[b]	Influent		Effluent	
	Range	Median	Range	Median
Total COD (mg/liter)	300–5,400	2,550	300–1,510	756
Soluble COD (mg/liter)	245–4,900	2,300	100–1,042	490
Ethanol (mg/liter)	200–1,800	850	nd[a]	nd
VFA (meq/liter)	0.1–24	13	0–12.6	1.6
TK-N (mg/liter)	9–137	48	14–276	44
NH_4^+-N (mg/liter)	1.2–59	8	5–87	10
PO_4^{3-} (mg/liter)	7.1–45	30	7–45	30
SO_4^{2-} (mg/liter)	0–120	5.5	0–120	5.5
SS (mg/liter)	10–1,013	190	0–4,770	255
Alkalinity (meq/liter)	0–25	5.4	9.7–35.5	22
pH	5.6–6.8	6.1	6.3–7.9	6.7
Temp (°C)			18–35	30.5

[a] nd, not detected.
[b] TK-N, total Kjeldahl nitrogen; SS, suspended solids.

Because of the distinctive cluster morphology of the aggregates observed in the brewery-treating EGSB system, the operation efficiency of the reactor and the characteristics of the aggregates were monitored for more than 1 year. In this paper, we report on the metabolic properties, physical-chemical characteristics, and microbial structure of these clustered anaerobic granular sludge aggregates.

MATERIALS AND METHODS

Source of biomass. Anaerobic granules were grown in a full-scale EGSB reactor (total and liquid volumes of 780 and 570 m^3, respectively) treating brewery wastewater (pH 5.6 to 6.8). The full-scale reactor had operated 2 years and was initially inoculated with 12,000 kg of a mixture of granular sludge originating from UASB reactors treating potato and sugar processing wastewater. The reactor operated at 25 to 30°C and had a hydraulic retention time of 2 h and a volumetric loading rate of 20 kg of COD/m^3-day, with a COD removal efficiency of 70 to 75%. Table 1 gives the chemical compositions of the brewery wastewater (influent) and the EGSB reactor effluent.

Metabolic characteristics. The metabolic characteristics of the sludge were characterized by measuring methane production rates from different substrates. Tests were conducted in duplicate in 3.0-liter plastic (polyvinyl chloride) continuously stirred batch reactors containing 2.5 liters of mineral medium as described by Gonzalez-Gil et al. (11). For each test, the batch reactors were inoculated with 1.5 to 2.0 g of volatile suspended solids (VSS)/liter of intact or dispersed granular sludge. Dispersed granular sludge was obtained by disrupting the granular structure with a blender (Braun 4164) for about 1 min. By sieving the dispersed sludge through metallic sieves, its size was determined as smaller than 200 μm. The substrate ethanol, acetate, or a volatile fatty acid (VFA) mixture (acetate-propionate-butyrate in a ratio of 1:1:1 on a COD basis) was added from concentrated stock solutions to give final concentrations of 1.5, 2, and 3 g of COD/liter, respectively. After addition of the substrate, the methane production rate was monitored on-line by measuring the weight of the liquid displaced by the methane produced with a pressure sensor connected to a programmable data logger system as described previously (11).

Stereomicroscopy. Low-magnification studies of EGSB aggregates were done using an Olympus SZ-PT stereomicroscope. Photographs were taken with an Olympus C-35AD-4 camera attached to the stereomicroscope.

SEM and elemental analyses. Scanning electron microscopy (SEM) was done with a scanning electron microscope (JSM 6300F; JEOL, Tokyo, Japan) at 5 kV. Intact and cross-sectioned granules were prepared as described by van Langerak et al. (43) except that fixation was for 3 h and samples were coated with 5 nm of platinum by magnetron sputtering.

The same sample preparation procedure was followed for energy-dispersed X-ray (EDX) analysis and back-scattered electron analysis, except that osmium tetraoxide was omitted and the platinum layer was replaced by a carbon coating (07160; Balzers, Balzers, Liechtenstein). EDX analysis, i.e., the detection of elements and their spatial distribution, was done for 12 h per sample (Voyager III; Noran, Middleton, Wis.) in the scanning electron microscope at 15 kV. Back-scattered SEM analysis is a special type of SEM which differentiates organic-rich and metal-rich zones within a sample. Electrons are back scattered in metal-rich zones, thus lighting up these zones (white in the image). In contrast, organic matter absorbs the electrons, resulting in black in the picture. To detect these mass differences on the surface of the aggregates, back-scattered electron detection (AutraDet, Brno, Czechoslovakia) was performed in the scanning electron microscope at 10 to 15 kV.

In situ hybridization. Fluorescence in situ hybridization (FISH) with rRNA-targeted oligonucleotide probes was used to assess the main microbial domains present in the aggregates. Crushed aggregates were fixed as described previously (34). The protocol described by Manz et al. (25) was used for the in situ hybridization of the crushed-aggregate biomass with probes ARC915 and EUB338 for detection of *Archaea* and eubacteria, respectively. The probe concentrations were 5 ng/ml, and hybridization was performed for 1 to 2 h at 46°C. Hybridized samples were microscopically examined with a Zeiss LSM 510 confocal laser scanning microscope (Carl Zeiss, Jena, Germany) equipped with two HeNe lasers (543 and 633 nm).

NMR imaging. Nuclear magnetic resonance (NMR) imaging allows nondestructive and noninvasive spatially resolved measurements of water transport processes within aggregates. NMR signals are characterized by a number of different parameters: (i) the amplitude A, a direct measure of the amount of water in a sample, and (ii) two relaxation times (T_1 and T_2) of the excited nuclear spin system, which both correlate with the physical state of water in the sample (41). Functional imaging and data processing to simultaneously obtain the A, spin-spin relaxation time T_2, and self-diffusion coefficient D were done using a pulsed-field gradient–Garr-Purcell-Meiboom-Gill sequence as described by Van Dusschoten et al. (42). Typical acquisition parameters were as follows: repetition time, 1 s; 4 averages; spectral width, 50 kHz; number of echoes, 64; echo time, 5 ms. The field of view was 10 mm with a slice thickness of 2 mm, yielding 128 by 128 voxels with a resolution of 80 by 80 by 2,000 μm^3. The PFG pulses had a duration of 2.5 ms. The observation time was 10 ms during which three 180° radio frequency excitation pulses were given with an interval of 3.1 ms. NMR measurements were done by placing a single unfed and degassed aggregate into a test tube filled with demineralized water. As a control, a small tube (outer diameter, 2 mm) containing demineralized water supplemented with $MnCl_2$ to reduce its T_2 was included in the test tube as well.

Physicochemical characteristics. The settling characteristics of the biomass were obtained from the evolution of the weight of the settled sludge as a function of the sedimentation time as described by Hulshoff Pol et al. (17). Granular strength was determined as the resistance against axial compression forces (17). The granular size distribution was analyzed by image analysis as described previously (11).

Analysis. The concentrations of total suspended solids and VSS and the specific gravity were determined by standard methods (1). VFA and CH_4 were determined by gas chromatography as described by Gonzalez-Gil et al. (11).

RESULTS

Physicochemical characteristics of the EGSB aggregates. The spherical aggregates were black but contained numerous whitish spots on their surfaces (Fig. 1A). Stereomicroscopy of

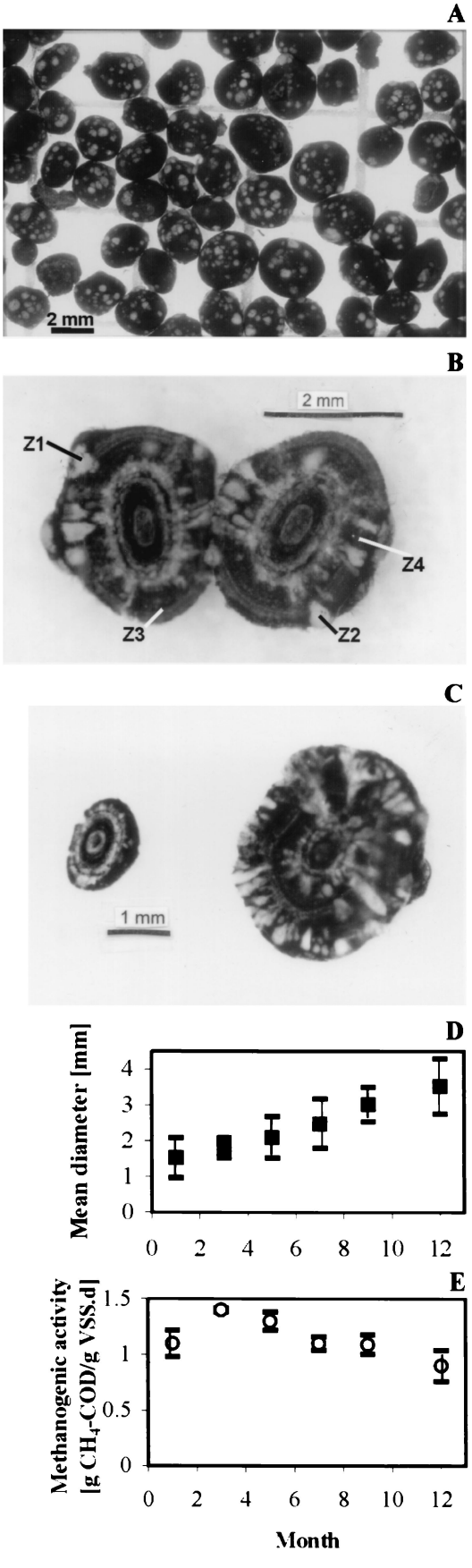

cross-sectioned aggregates showed that these whitish spots corresponded to clusters coming from the interior of the aggregates (Fig. 1B). The aggregates clearly increased in size over the 1-year period (Fig. 1C), with their mean diameter increasing from 1.5 to 3.5 mm during the 1-year reactor operation (Fig. 1D). Interestingly, the white clusters developed simultaneously with the increase in diameter (Fig. 1C).

The mean density of the aggregates was 1,037 kg/m^3. The aggregates had a rather low ash content (about 15%), which did not vary much during the 1 year of reactor operation. The mean settling velocity was 50 m/h, which increased to about 75 m/h over the 1-year period of reactor operation. The average strength of the aggregates was 300 ± 60 kN/m^2, but a clear increase up to 400 kN/m^2 was observed during the first 6 months of operation.

Activity with VFA as the substrates. The sludge had an average maximal specific methanogenic activity on acetate of 1.1 g of CH_4 COD/g of VSS·day (Fig. 1E). This maximum specific activity increased to about 1.4 g of CH_4 COD/g of VSS·day during the first months of reactor operation but gradually decreased to 0.9 g of CH_4 COD/g of VSS·day during the last months of operation.

Figure 2A and B show the methane production rate from the simultaneous conversion of acetate, propionate, and butyrate. The shape of the methane production rate changed over time, corresponding to the sequential degradation of acetate, propionate, and butyrate. The methane production rate during days 0 to 1 confirms the high acetate conversion capacity of the sludge. The maximum methanogenesis from acetate of intact EGSB aggregates (Fig. 2A) was similar to that of crushed EGSB aggregates (Fig. 2B).

Initial methanogenesis from propionate and butyrate was very low (Fig. 2A and B). The exponential increase of the methane production rate after about 4 days of incubation corresponds to the simultaneous metabolism of butyrate and propionate. This suggests the proliferation of butyrate- and propionate-degrading consortia during the activity test. The crushed sludge had a much steeper butyrate consumption rate and consequently steeper methane production curves (Fig. 2B versus A), suggesting mass transfer limitation for butyrate in the intact biomass. Also less H_2 accumulated in the batch test with crushed sludge (Fig. 2B versus A). Acetate could not be detected during the conversion of the two higher VFA (Fig. 2A and B), which agrees with the high acetate conversion capacity of the sludge. The highest methane production rate (65 mmol/liter·day [4 g of COD/liter·day]) was obtained when formate was added as the substrate (data not shown).

Activity with ethanol. Figure 2C shows the methane production rate following the addition of the substrate ethanol to crushed aggregates. As reactivation, a first feed of acetate (F1)

FIG. 1. Morphology and sizes of the EGSB aggregates. (A) Overview of a sludge sample taken on the 5th month of reactor operation. (B) Cross section of an aggregate from the 7th month. Z1 to Z4, locations of microscopic observations presented in Fig. 5. (C) Comparison of granules from the start (left granule) and end (right granule) of the 1-year study period. (D) Development of the mean diameter of the granular sludge over the 1-year period. (E) Evolution of the specific methanogenic activity on acetate as a function of time.

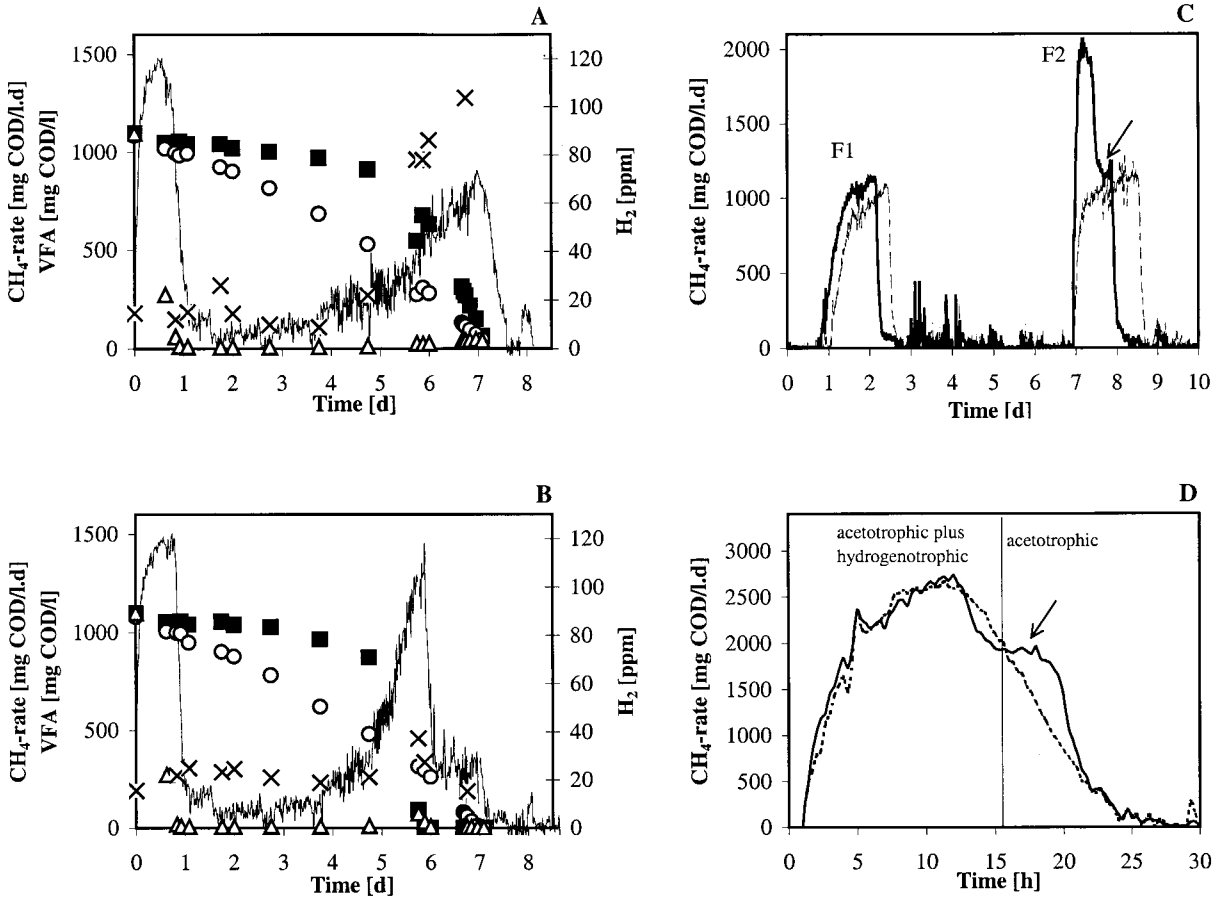

FIG. 2. Metabolic properties of the EGSB aggregates. (A and B) Methane production rates (lines) from a mixture of acetate (△), propionate (○), and butyrate (■) by granular sludge (A) and crushed granular sludge (B). ×, hydrogen. (C) Methane production rate of crushed aggregates. The first substrate feed (F1) consisted of ~1,000 mg of acetate COD/liter, and the second substrate feed (F2) consisted of ~1,500 mg of ethanol COD/liter added to one batch reactor (solid line) and ~1,500 mg of acetate COD/liter added to a second batch reactor (dashed line). (D) Methane production rates from ethanol by intact (dashed line) and crushed (solid line) aggregates. Arrow (C and D), tailing on the methane production rate curve from the crushed biomass due to acetotrophic methanogenesis.

was applied to the batch reactors. F1 was followed by a second feed (F2) of ethanol to one batch reactor, while acetate was added again to the other batch reactor. Ethanol conversion to methane and carbon dioxide includes, besides the conversion of acetate to methane and carbon dioxide (acetotrophic methanogenesis), the conversion of hydrogen and carbon dioxide to methane (hydrogenotrophic methanogenesis). It should be noted that ethanol conversion can also proceed via propionate as an intermediate (20). However, the latter route is unlikely to be important for ethanol conversion since no propionate could be detected during the incubation (data not shown) and since the propionate conversion rates of the sludge were very low (Fig. 2A and B). Thus, by comparing (by subtraction) the methane production rate of the acetate-fed reactor with that of the ethanol-fed reactor, it is possible to estimate the contribution of hydrogenotrophic methanogenesis to the total methanogenesis from ethanol. Nearly at the end of the test of the ethanol-fed batch reactor a "tailing" on the methane production rate was observed (Fig. 2C). The methane production rate from this tailing is mainly due to methanogenesis from acetate since it coincides with the methane production rate of the batch reactor fed only with acetate.

The maximum methane production rate from ethanol for crushed EGSB aggregates was similar to that for intact EGSB aggregates (Fig. 2D). From about 15 h after ethanol addition until the end of the test, most of the methane produced was due to the conversion of acetate. This is confirmed by ethanol and acetate analyses (data not shown) that indicated that the methane production from day 7.5 (Fig. 2C) and 15 h (Fig. 2D) until the end of the experiments was due to methanogenesis from acetate. The methane production rate of the crushed biomass between 17 and 20.5 h (Fig. 2D) was higher than that of the intact aggregates, which may be due to mass transfer limitations for acetate in the intact aggregates. Internal mass transfer limitations for acetate of these EGSB aggregates have been clearly demonstrated in a previous study (11).

Chemical structure of the EGSB aggregates. Initially, the whitish clusters observed under stereomicroscopy were thought to be inorganic precipitates, e.g., $CaCO_3$ or calcium phosphate. Since bicarbonate is produced during anaerobic

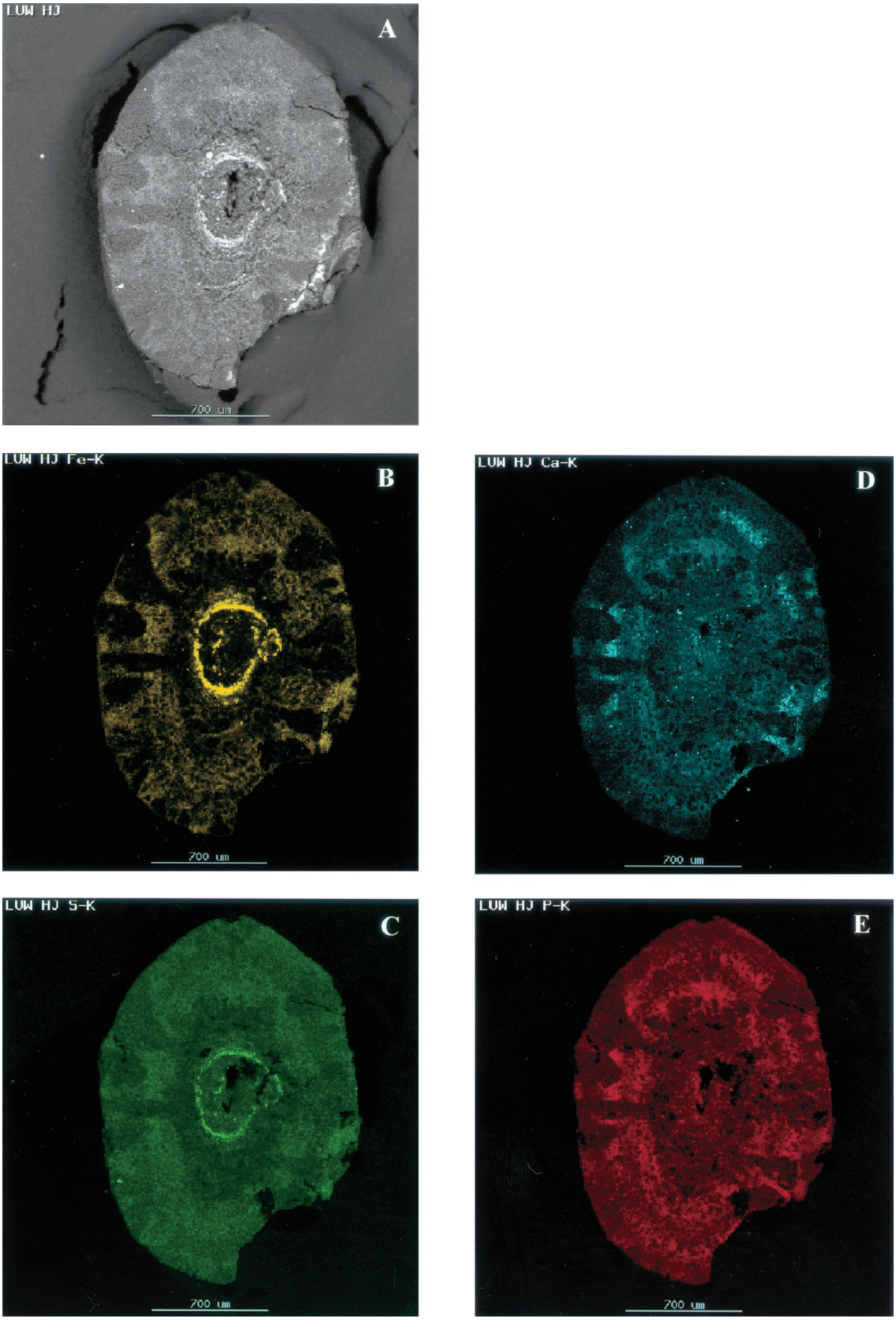

FIG. 3. EDX analysis of a cross-sectioned aggregate. (A) Back-scattered electron image from which mappings of iron (B), sulfur (C), calcium (D), and phosphorus (E) were made. Note that the deposition of metals corresponds to the light areas observed in the back-scattered electron image.

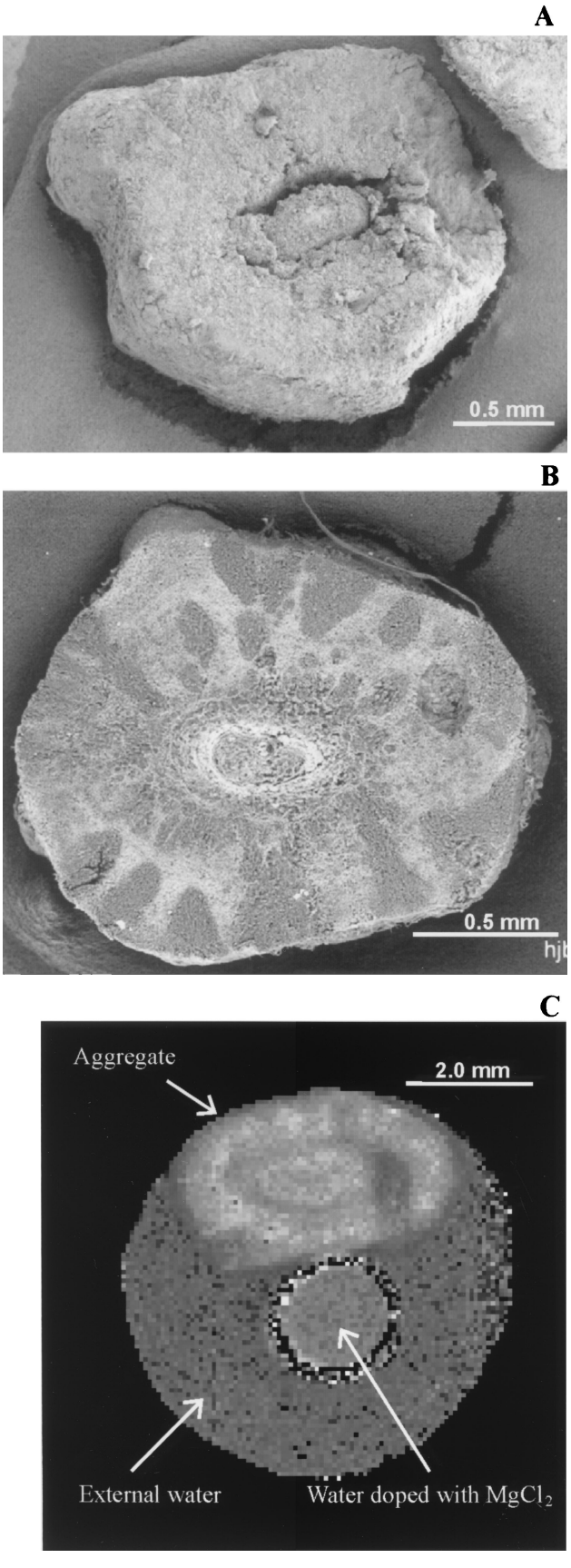

conversion of acetate, calcium precipitates can form within the sludge, even at reactor calcium concentrations as low as 200 mg/liter (13, 40). $CaCO_3$ precipitates are white. However, EDX analysis of cross-sectioned granules (Fig. 3) showed that there was no correlation between the location of the whitish clusters and high Ca (Fig. 3D) or P (Fig. 3E) concentrations. In contrast, Fe predominated in the black zones (Fig. 3B).

To further characterize the chemical composition of the whitish clusters, cleaved aggregates were subjected to back-scattered SEM image analysis. Normal SEM uses samples that are sputter coated with platinum, an element of high atomic mass known to interfere with the emission of the electrons from the surface of the sample. Thus, different zones (i.e., whitish spots) observed under stereomicroscopy (Fig. 1B) are masked by normal SEM (Fig. 4A). When no platinum is used, the sample can be observed with back-scattered electrons. In this way, different zones with different chemical compositions can be recognized (Fig. 4B). The dark areas indicate regions with high concentrations of elements of low atomic mass (for example, carbon), whereas the light areas indicate regions rich in elements of high atomic mass (e.g., metals). The back-scattered images (Fig. 4B) suggested that the whitish clusters of the sludge (dark under back-scattered SEM) contained a much higher biomass concentration (indicated as higher carbon content) than the black zones.

Physical structure of the EGSB aggregates. The NMR image (Fig. 4C) of spin-spin relaxation rate R_2 ($= 1/T_2$) also distinguished the white and black zones observed under stereomicroscopy (Fig. 1B). This means that water in the white clusters is present in a physically different state (e.g., smaller micropores, higher polymer density) than in the black zones. The cluster morphology could also distinguished in the self-diffusion coefficient image, although the contrast-to-noise ratio was much lower than in the R_2 image (data not shown). Using image-processing tools, zones with a particular R_2 value were selected in the self-diffusion coefficient image, and the average effective diffusion coefficient of such a group of pixels was calculated. The apparent diffusion coefficient in the whitish clusters (53% ± 7% of the self-diffusion coefficient of free water) was significantly lower than that in the dark zones (73% ± 10% of the self-diffusion of free water), indicating that diffusional transport in the whitish zones was significantly slower than that in the black matrix.

Microbiological structure of the EGSB aggregates. The FISH analyses with probes ARC915 and EUB338 detected on average 70 and 30%, respectively, of the DAPI (4′,6-diamino-2-phenylindole)-stained cells. About 1 to 5% of the DAPI-

FIG. 4. (A) SEM image of a cross-sectioned aggregate. The oval structure at the center is most likely the original seed sludge. (B) Cross-sectioned aggregate observed with back-scattered SEM showing the cluster-like arrangement of the EGSB aggregate. Dark areas, regions with higher biomass concentrations; light areas, regions with high metal content. (C) Map of spin-spin relaxation rate R_2 ($= 1/T_2$) for a test tube containing a single (intact) EGSB aggregate immersed in demineralized water and a reference tube filled with $MnCl_2$-doped demineralized water. Spatial resolution of the T_2 map, 80 μm; slice thickness, 2 mm. White areas, regions with a high R_2, i.e., slow relaxation rate. Note that R_2 is the result of the physicochemical environments, i.e., pore size or polymer density (41).

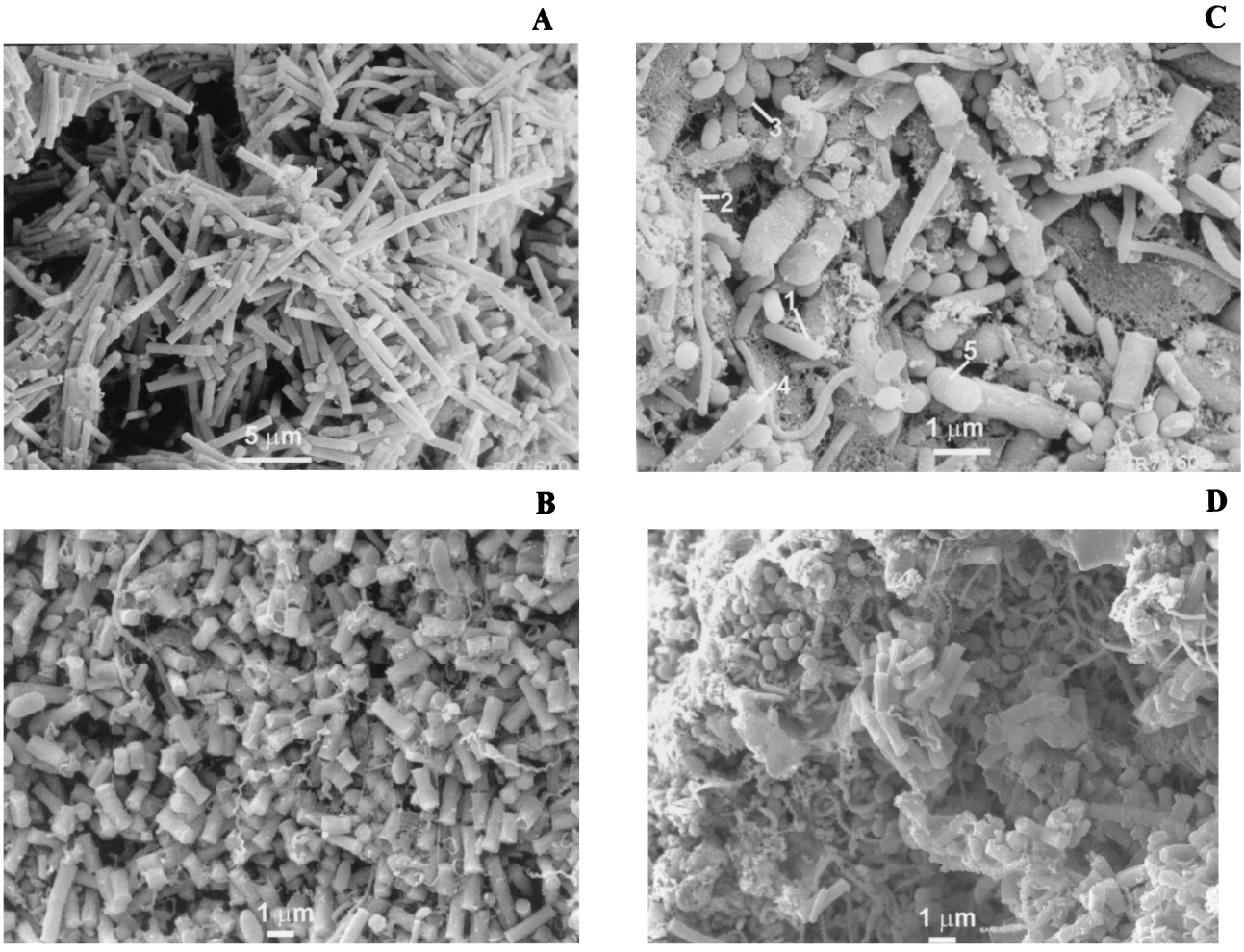

FIG. 5. SEM images taken from zones indicated in Fig. 1B. Images were obtained from cluster zones Z1 (A) and Z2 (B) and from areas between clusters Z3 (C) and Z4 (D). In the cluster zones mainly *Methanosaeta*-like microorganisms were observed, while in the areas between the clusters a more heterogeneous population was observed including methanogens, i.e., *Methanobacterium*-like (1), *Methanospirillum*-like (2), and *Methanococcus*-like (3) organisms, as well as syntrophs, a *Pelobacter*-like ethanol oxidizer (4), and a likely propionate oxidizer (5).

stained cells hybridized to probe SRB385 (data not shown), suggesting that, despite the low sulfate concentration in the influent (Table 1), the sludge also contained a substantial population of sulfate-reducing bacteria.

High-magnification SEM showed that different bacterial densities and populations inhabited the light and dark zones. In the whitish zone (i.e., zones with very high biomass concentration), predominantly *Methanosaeta*-like organisms were present, either in filamentous (Fig. 5A) or single-rod form (Fig. 5B). In contrast, the black regions (i.e., zones with higher metal content) contained several bacterial morphologies. Microorganisms resembling *Methanobacterium* and *Methanospirillum*, both hydrogen- and formate-consuming methanogens, and ethanol-oxidizing *Pelobacter*-like bacteria (Fig. 5C and D) could be distinguished.

DISCUSSION

This paper reports on methanogenic aggregates with a cluster morphology grown in a full-scale EGSB reactor treating brewery wastewater. This is to the best of our knowledge the first report of anaerobic aggregates containing such a cell cluster morphology. The mechanism leading to the development of this morphology in this particular EGSB sludge is not resolved. It is clear, though, that the interrelation between hydrodynamic conditions, substrate composition and/or concentration, and the microorganisms' kinetic properties plays a key role.

The clusters can develop as the outcome of solely physical aspects associated with space limitation for microorganisms when growing in a biofilm. When cells divide, daughter cells take up a volume element as well, thus pushing away neighboring cells. This can be unidirectional (31) or multidirectional or can occur by shoving (19). Model simulations of aerobic biofilms using either of these mechanisms yield cluster formation for substrate transport-limited conditions (29). In contrast, compact and dense biofilms develop in systems limited by the biomass growth rate (29–31). When a nutrient gets depleted in the deeper layers of the biofilm or aggregate, only microbes in the top regions are actively dividing and creating new biomass. Thus, biofilm or aggregate growth becomes unidirectional and colonies grow as "fingers" toward the liquid bulk (29, 31).

The arrangement of a cluster (i.e., white zones) and a porous

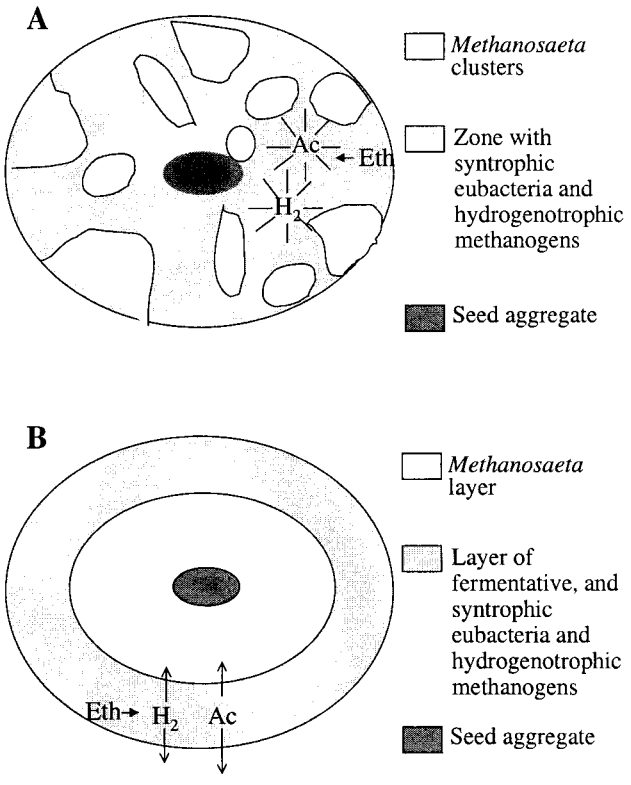

FIG. 6. Schematic representation of the architecture of anaerobic aggregates. (A) Cluster-like arrangement; (B) layered arrangement. Note that in both cases acetate-utilizing *Methanosaeta* organisms segregate from the other microbiota. Ac, acetate; Eth, ethanol.

matrix (i.e., dark zones) can also be the microbiological response to the specific in situ conditions prevailing in aggregates. It has been suggested that cell-free channel structures may be a microbial strategy to deal with the problem of limited diffusional transport in thick aerobic heterogeneous biofilms in trickling filters (33) and fluidized-bed reactors (26). Since low substrate concentrations are maintained in EGSB reactors (Table 1), the observed cluster arrangement of the EGSB aggregates may indeed be the result of transport-limiting conditions. It is, however, unlikely that this is the sole determining factor, as the cluster morphology has thus far not been reported in other EGSB or UASB reactors, many of them operating at effluent concentrations below 0.2 g of COD/liter.

TABLE 2. Comparison of the maximum specific activity on acetate of the EGSB sludge with different substrates to that of a full-scale UASB granular sludge treating brewery wastewater

Substrate	Maximum CH_4 production rate (g of CH_4 COD/g of VSS · day) for:		Reference or source
	Granules	Dispersed sludge	
Acetate	1.1	1.1	This study
	0.51	—[a]	45
Formate	—	2.1	This study
	0.86	2.35	45
Ethanol	1.25	1.25	This study
	1.9	—	45

[a] —, not available.

The cluster arrangement described here might also be the optimal cell arrangement for syntrophic associations. Anaerobic degradation of ethanol, the main component of brewery wastewater, to acetate and H_2 is thermodynamically unfavorable under standard conditions (Gibbs free energy [$\Delta G^{o'}$] = +9.6 kJ/mol). The reaction only proceeds with the syntrophic association of ethanol-acetogenic H_2-producing bacteria (e.g., *Pelobacter* sp. or sulfate-reducing bacteria in the absence of sulfate) and both hydrogenotrophic and acetoclastic methanogens (35). The reaction can become exergonic when the concentration of the reaction product H_2 is low (35, 38), and many papers report on the cell-cell contact or juxtaposition between acetogens and hydrogen-utilizing methanogens as a prerequisite for syntrophic ethanol (38) or propionate (14, 15, 18, 36) degradation. Figure 5C and D show that this was also the case for the EGSB aggregates described in this study, since the black zones of the aggregates contained both syntrophic acetogens (converting ethanol to acetate and H_2-CO_2 and/or formate) and H_2- and formate-utilizing *Methanobacterium*-like and *Methanospirillum*-like methanogens. Note that the two methanogens cannot utilize acetate. Moreover, their apparent half-saturation constants (K_Ss) for H_2, ranging between 3×10^{-6} and 0.0375 mM (4.8×10^{-5} and 0.6 mg of COD/liter) (28), are much lower than the K_S of *Methanosaeta* for acetate, about 0.47 mM (30 mg of COD/liter) (47). Note also that *Methanosaeta* spp. are unable to utilize H_2-CO_2.

The fact that the white clusters almost exclusively contained *Methanosaeta* spp., methanogens which only utilize acetate, suggests that the clusters play a key role in acetate removal. Figure 6 shows that the cluster structure of EGSB aggregates may be an advantage for high-rate syntrophic ethanol conversion. Acetate produced in the black zones is transported by random diffusion in all directions and thus penetrates the *Methanosaeta* clusters from all sides. Hence, substrate-depleted zones are circumvented, which allows the growth of more active biomass per unit area of aggregate. This is in agreement with back-scattered SEM (Fig. 4B) and NMR imaging (Fig. 4C), which showed that the white *Methanosaeta* clusters had a higher density than the black multispecies matrix.

A layered microbial architecture as presented in Fig. 6B has been proposed when carbohydrates (15, 24) are the primary substrate. In this layered model, syntrophic microorganisms and acetoclastic methanogens (i.e., *Methanosaeta* spp.) are found, respectively, in the outer and inner layers of glucose-grown UASB aggregates. In contrast, in this study, a cluster arrangement was observed for brewery (ethanol-fed) EGSB aggregates. Figure 6B shows that the layered arrangement is a less effective way to scavenge acetate and H_2-CO_2 and/or formate, since a larger fraction of these compounds diffuses out of the biofilm. The cluster arrangement leads to less mass transfer limitation problems and reduced zones with very low or no substrate. Hence less zones with inactive or dead biomass might be present than are found with a layered arrangement. Compared to the clustered model (Fig. 6A), this situation might not be a problem in systems with a high bulk substrate

concentration, where, as mentioned above, compact and dense biofilms develop (29–30); these biofilms favor the development of a layered structure.

A last hypothesis to explain the observed cluster morphology is that, analogous to what is found for aerobic biofilms, anaerobes also produce cell-to-cell signaling molecules. Indeed, homoserine lactones and furanones can induce the creation of pores and channels within aerobic *Pseudomonas aeruginosa* biofilms (4, 5). Alternatively, these signaling molecules or their structural analogs might have been present in the wastewater, thus inducing cluster formation both in growing and newly formed anaerobic aggregates. This warrants further research on the identification of such signaling molecules and the factors that induce their formation in anaerobic environments.

Table 2 compares the specific methanogenic activity of EGSB aggregates with different substrates to that of other aggregates developed in full-scale UASB systems treating brewery wastewater. The activities with formate and ethanol are comparable for both types of aggregates (Table 2). However, the methanogenic activity of the EGSB granules with acetate (17.19 mmol of CH_4/g of VSS·day [1.1 g of CH_4 COD/g of VSS·day]) is about twofold higher. The maximum specific methanogenic activity reported in the literature on acetate of sludge from brewery full-scale UASB reactors ranges between 4.69 and 9.38 mmol of CH_4/g of VSS·day [0.3 to 0.6 g of CH_4 COD/g of VSS·day] (2, 9, 44, 45), which is also less than one-half of the activity of the aggregates described in this study. Thus, it is possible that the cluster architecture of the aggregates represents an optimal arrangement for the in- and outflux of substrate and gas products, respectively.

ACKNOWLEDGMENTS

This work was supported by Biothane Systems International, Delft, The Netherlands.

We thank F. Vergeldt and J. Sipma for assistance with the NMR and FISH analyses, respectively. The NMR measurements were supported by a grant of the EU Large Scale Facility Wageningen NMR center (ERBCHGECT 940061).

REFERENCES

1. **American Public Health Association.** 1985. Standard methods for examination of water and wastewater, 16th ed. American Public Health Association, Washington, D.C.
2. **Colleran, E., F. Concannon, T. Golden, F. Geoghegan, B. Crumlish, E. Killilea, M. Henry, and J. Coates.** 1992. Use of methanogenic activity test to characterize anaerobic sludges, screen for anaerobic biodegradability and determine toxicity thresholds against individual anaerobic trophic groups and species. Water Sci. Technol. **25:**31–40.
3. **Costerton, J. W., Z. Lewandowski, D. De Beer, D. Caldwell, D. Korber, and G. James.** 1994. Biofilms, the customized microniche. J. Bacteriol. **176:**2137–2142.
4. **Davey, M. E., and G. A. O'Toole.** 2000. Microbial biofilms: from ecology to molecular genetics. Microbiol. Mol. Biol. Rev. **64:**847–867.
5. **Davies, D. G., M. R. Parsek, J. P. Pearson, B. H. Iglewski, J. W. Costerton, and E. P. Greenberg.** 1998. The involvement of cell-to-cell signals in the development of a bacterial biofilm. Science **280:**295–298.
6. **De Beer, D., P. Stoodley, and Z. Lewandowski.** 1996. Liquid flow and mass transport in heterogeneous biofilms. Water Res. **30:**2761–2765.
7. **De Beer, D., P. Stoodley, and Z. Lewandowski.** 1994. Liquid flow in heterogeneous biofilms. Biotechnol. Bioeng. **44:**636–641.
8. **Dolfing, J., A. Griffioen, A. van Neerven, and L. Zevenhuizen.** 1985. Chemical and bacteriological composition of granular methanogenic sludge. Can. J. Microbiol. **31:**744–750.
9. **Fang, H. H. P., H. K. Chui, and Y. Y. Li.** 1995. Microstructural analysis of UASB granules treating brewery wastewater. Water Sci. Technol. **31:**129–135.
10. **Gjaltema, A., P. A. M. Arts, C. M. C. van Loosdrecht, and J. J. Heijnen.** 1994. Heterogeneity of biofilms in rotating annular reactors: occurrence, structure and consequences. Biotechnol. Bioeng. **44:**194–204.
11. **Gonzalez-Gil, G., L. Seghezzo, G. Lettinga, and R. Kleerebezem.** 2001. Kinetics and mass-transfer phenomena in anaerobic granular sludge. Biotechnol. Bioeng. **73:**125–134.
12. **Grotenhuis, J. T. C., M. Smit, C. M. Plugge, X. Yuansheng, A. A. M. van Lammeren, A. J. M. Stams, and A. J. B Zehnder.** 1991. Bacterial composition and structure of granular sludge adapted to different substrates. Appl. Environ. Microbiol. **57:**1942–1949.
13. **Guiot, S. R., S. Rochelau, J. Hawari, and R. Samson.** 1992. Induction of granulation by sulphonated-lignin and calcium in an upflow anaerobic sludge bed reactor. J. Chem. Technol. Biotechnol. **53:**45–56.
14. **Harmsen, H. J. M., A. D. L. Akkermans, A. J. M. Stams, and W. M. de Vos.** 1996. Population dynamics of propionate-oxidizing bacteria under methanogenic and sulfidogenic conditions in anaerobic granular sludge. Appl. Environ. Microbiol. **62:**2163–2168.
15. **Harmsen, H. J. M., H. M. P. Kengen, A. D. L. Akkermans, A. J. M. Stams, and W. M. de Vos.** 1996. Detection and localization of syntrophic propionate-oxidizing bacteria in granular sludge by in situ hybridization using 16S rRNA-based oligonucleotide probes. Appl. Environ. Microbiol. **62:**1656–1663.
16. **Huang, C. T., K. D. Xu, G. McFeters, and P. S. Stewart.** 1998. Spatial patterns of alkaline phosphatase expression within bacterial colonies and biofilms in response to phosphate starvation. Appl. Environ. Microbiol. **64:**1526–1531.
17. **Hulshoff Pol, L. W., J. J. M. Van de Worp, G. Lettinga, and W. A. Beverloo.** 1986. Physical characterization of anaerobic granular sludge. *In* Proceedings of NVA-EWPCA Water Treatment Conference. Industrial Presentations (Europe) B. V., Schiedam, The Netherlands.
18. **Imachi, H., Y. Sekiguchi, Y. Kamagata, A. Ohashi, and H. Harada.** 2000. Cultivation and in situ detection of a thermophilic bacterium capable of oxidizing propionate in syntrophic association with hydrogenotrophic methanogens in a thermophilic methanogenic granular sludge. Appl. Environ. Microbiol. **66:**3608–3615.
19. **Kreft, J. U., G. Booth, and J. W. T. Wimpenny.** 1998. BacSim, a simulator for individual-based modelling of bacterial colony growth. Microbiology **144:**3275–3287.
20. **Laanbroek, H. J. T., T. Abee, and I. L. Voogd.** 1982. Alcohol conversions by Desulfobolus propionicus Lindhorst in the presence and absence of sulfate and hydrogen. Arch. Microbiol. **133:**178–184.
21. **Lens, P. N. L., D. de Beer, C. C. H. Cronenberg, F. P. Houwen, S. P. P. Ottengraef, and W. Verstraete.** 1993. Heterogeneous distribution of microbial activity in methanogenic aggregates: pH and glucose microprofiles. Appl. Environ. Microbiol. **59:**3803–3815.
22. **Lettinga, G.** 1995. Anaerobic digestion and wastewater treatment systems. Antonie Leeuwenhoek **67:**3–28.
23. **Lewandowski, Z., G. Walser, and W. G. Characklis.** 1991. Reaction kinetics in biofilms. Biotechnol. Bioeng. **38:**877–882.
24. **MacLeod, F. A., S. R. Guiot, and J. W. Costerton.** 1990. Layered structure of bacterial aggregates produced in an upflow anaerobic sludge bed and filter reactor. Appl. Environ. Microbiol. **56:**1598–1607.
25. **Manz, W., R. Amann, W. Ludwig, M. Wagner, and K. H. Schleifer.** 1992. Phylogenetic oligodeoxynucleotide probes for the major subclasses of proteobacteria: problems and solutions. Syst. Appl. Microbiol. **15:**593–600.
26. **Massol-Deya, A. A., J. Whallon, R. F. Hickey, and J. M. Tiedje.** 1995. Channel structures in aerobic biofilms of fixed-film reactors treating contaminated groundwater. Appl. Environ. Microbiol. **61:**769–777.
27. **Nicolella, C., M. C. M. van Loosdrecht, and S. J. Heijnen.** 2000. Particle-based biofilm reactor technology. Tibtechnology **18:**312–320.
28. **Pavlostathis, S. G., and E. Giraldo-Gomez.** 1991. Kinetics of anaerobic treatment: a critical review. Crit. Rev. Environ. Control **21:**411–490.
29. **Picioreanu, C., M. C. M. van Loosdrecht, and J. J. Heijnen.** 1998. Mathematical modeling of biofilm structure with a hybrid differential-discrete cellular automaton approach. Biotechnol. Bioeng. **58:**101–116.
30. **Picioreanu, C., M. C. M. van Loosdrecht, and J. J. Heijnen.** 1999. Discrete-differential modeling of biofilm structure. Water Sci. Technol. **39:**115–122.
31. **Picioreanu, C., M. C. M. van Loosdrecht, and J. J. Heijnen.** 2000. Effect of diffusive and convective substrate transport on biofilm structure formation: a two-dimensional modeling study. Biotechnol. Bioeng. **69:**504–515.
32. **Rittmann, B. E., and J. A. Manem.** 1992. Development and experimental evaluation of a steady-state, multispecies biofilm model. Biotechnol. Bioeng. **39:**914–922.
33. **Rittmann, B. E., M. Pettis, H. W. Reeves, and D. A. Stahl.** 1999. How biofilm clusters affect substrate flux and ecological selection. Water Sci. Technol. **39:**99–105.
34. **Santegoeds, C. M., L. R. Damgaard, G. Hesselink, J. Zopfi, P. Lens, G. Muyzer, and D. De Beer.** 1999. Distribution of sulfate-reducing and methanogenic bacteria in anaerobic aggregates determined by microsensor and molecular analysis. Appl. Environ. Microbiol. **65:**4618–4629.
35. **Schink, B.** 1997. Energetics of syntrophic cooperation in methanogenic degradation. Microbiol. Mol. Biol. Rev. **61:**262–280.
36. **Schink, B., and R. K. Thauer.** 1988. Energetics of syntrophic methane formation and the influence of aggregation, p. 5–17. *In* G. Lettinga et al. (ed.),

Granular anaerobic sludge: microbiology and technology. Pudoc, Wageningen, The Netherlands.
37. **Sekiguchi, Y., Y. Kamagata, K. Nikamura, A. Ohashi, and H. Harada.** 1999. Fluorescence in situ hybridization using 16S rRNA-targeted oligonucleotides reveals location of methanogens and selected uncultured bacteria in meshophilic and thermophilic sludge granules. Appl. Environ. Microbiol. **65:**1280–1288.
38. **Stams, A. J. M.** 1994. Metabolic interactions between anaerobic bacteria in methanogenic environments. Antonie Leeuwenhoek. **66:**271–294.
39. **Stoodley, P., J. D. Boyle, D. De Beer, and H. M. Lappin-Scott.** 1999. Evolving perspectives of biofilm structure. Biofouling **14:**75–90.
40. **Uemura, S., and H. Harada.** 1995. Inorganic composition and microbial characteristics of methanogenic granular sludge grown in a thermophilic upflow anaerobic sludge blanket reactor. Appl. Microbiol. Biotechnol. **43:** 358–364.
41. **Van As, H., and P. N. L. Lens.** 2001. Use of 1H NMR to study transport processes in porous biosystems. J. Ind. Microbiol. Biotechnol. **26:**43–52.
42. **Van Dusschoten, D., P. A. De Jager, and H. Van As.** 1995. Extracting diffusion constants from echo-time-dependent PFG NMR data using relaxation-time information. J. Magn. Reson. Ser. A **116:**22–28.
43. **van Langerak, E. P. A., G. Gonzalez-Gil, A. Van Aelst, J. B. van Lier, H. V. M. Hamelers, and G. Lettinga.** 1998. Effects of calcium concentrations on the development of methanogenic sludge in UASB reactors. Water Res. **32:**1255–1263.
44. **Wu, M. M., C. Criddle, and R. Hickey.** 1995. Mass transfer and temperature effects on substrate utilization by brewery granules. Biotechnol. Bioeng. **46:**465–475.
45. **Wu, W. M., R. Hickey, and J. G. Zeikus.** 1991. Characterization of metabolic performance of methanogenic granules treating brewery wastewater: role of sulfate-reducing bacteria. Appl. Environ. Microbiol. **57:**3438–3449.
46. **Yang, S., and Z. Lewandowski.** 1995. Measurement of local mass transfer coefficient in biofilms. Biotechnol. Bioeng. **48:**737–744.
47. **Zehnder, A. J. B., B. A. Huser, T. D. Brock, and K. Wuhrmann.** 1980. Characterization of an acetate-decarboxylating, non-hydrogen-oxidizing methane bacterium. Arch. Microbiol. **124:**1–11.
48. **Zoutberg, G. R., and R. Frankin.** 1996. Anaerobic treatment of chemical and brewery wastewater with a new type of anaerobic reactor: the Biobed EGSB reactor. Water Sci. Technol. **34:**375–381.